

# Aerodynamic Effects of Strake Patterns on Flow around a Yawed Circular Cylinder

DongHun Yeo <sup>a</sup>, Nicholas P. Jones <sup>b</sup>

<sup>a</sup>*National Institute of Standards and Technology, Gaithersburg, MD, U.S.A., donghun.yeo@nist.gov*

<sup>b</sup>*Johns Hopkins University, Baltimore, MD, U.S.A., npjones@jhu.edu*

**ABSTRACT:** Strakes on a circular cylinder effectively mitigate Kármán vortex induced vibration of a cylinder normal to flow and have been applied to reduction of large-amplitude vibrations of a stay cable in cable-stayed bridges, which occur under wind oblique to a cable with or without rainfall. This aerodynamic approach cannot be fully effective without understanding behavior of flow around and the associated forces on an oblique cable. To address this issue, flow around a yawed cylinder with various strake patterns was studied using three-dimensional detached eddy simulation. Results demonstrated that strake patterns strongly influence the development of flow structures around a yawed cylinder and therefore the associated forces on the cylinder. The results suggest that particular strake patterns are able to provide an aerodynamic approach that mitigates large-amplitude and low-frequency vibrations of stay cables induced by oblique wind.

## 1 INTRODUCTION

Large-amplitude cable vibrations cause concerns with both safety and serviceability of cable-stayed bridges. These vibrations have been frequently observed since the first report of the vibrations with rain in 1998 (Hikami and Shiraishi, 1988). They are generally known as “rain-wind induced vibrations” because of their common occurrence with rain, but they have been also observed in the absence of precipitation (Main and Jones, 1999; Matsumoto et al., 1998). These oscillations have much lower frequencies and larger amplitudes than the classical Kármán vortex-induced vibrations in the same wind environment.

To mitigate this problem, mechanical and aerodynamic approaches have been proposed and applied to bridges. They require additional investment in constructing and maintaining the countermeasures (e.g., dampers.). However, they cannot be fully effective without taking advantage of knowledge of the fundamental mechanisms of the wind-induced vibrations. If the mechanism is understood, an aerodynamic approach that addresses the *cause* will likely lead to a more economical mitigation strategy.

Excitation mechanisms suggested by various researchers can be categorized into high speed vortex-induced vibration or galloping instability. The former is related to a velocity-restricted response (Matsumoto, 1998), and the latter is related to flow instability due to water rivulet (Hikami and Shiraishi, 1988; Verwiebe and Ruscheweyh, 1998) or due to cable inclination (Larose et al., 2003). However, the approaches employed in the studies above were two-dimensional or equivalent. The authors recently suggested a mechanism of force generation where the forces induced by oblique wind develop three-dimensionally on a circular cylinder (Yeo and Jones, 2009). It showed that a series of moving forces at spatial interval are generated under a specific range of yaw angles when Kármán vortex shedding around a yawed cylinder is mitigated due to the obliqueness of the cylinder to the flow. The low-frequency forces are trans-

mitted along the cylinder axis using modulation of frequency and amplitude of forces. The mitigated Kármán vortex shedding is a necessary condition for generation of the low-frequency moving forces. Therefore, an aerodynamic countermeasure should be effective when Kármán vortex shedding is fully suppressed around a yawed cylinder, and disturbance of the force generation mechanism can be also successful. Modification of a cross section is one approach. Various patterns, such as spiral strakes or helical fillets, have been used in the past mitigation strategies, but their deployment has generally not been based on analytical or computational studies or rational design procedures (Matsumoto, 1998; Miyata et al., 1994).

The goal of this study is to begin the development of an approach using a suitable defined strake pattern to effectively reduce the low-frequency forces induced by oblique wind. This paper focuses on understanding effects of strake patterns on the three-dimensional characteristics of flow around, and the associated forces on, a yawed circular cylinder.

## 2 NUMERICAL SIMULATION

### 2.1 *Spalart-Allmaras DES approach*

Detached eddy simulation (DES), developed by Spalart et al. (1997), is a hybrid approach to turbulence modeling of large eddy simulation (LES) and Reynolds averaged Navier-Stokes simulation (RANS). The Spalart-Allmaras DES approach employs a conventional RANS approach in the boundary layers near a wall, but uses LES-like approach in the separated flow away from a wall by modifying the Spalart-Allmaras RANS turbulence model (Spalart and Allmaras, 1992). This hybrid technique allows unsteady three-dimensional computations at high Reynolds number while maintaining manageable computational requirements (Spalart, 2000).

### 2.2 *Angles and coordinates of a yawed cylinder*

Figure 1 shows a yaw angle, global coordinates of computational domain, and local coordinates of a yawed cylinder used in this study. The incoming flow goes from left to right. The yaw angle  $\beta$  is defined as the angle from an axis oriented normal to the incoming flow (line AB) to a horizontally skewed cylinder (line AC). The global coordinates consist of  $X$  axis in the direction of the incoming flow,  $Y$  axis in the upward direction normal to the plane ABC, and  $Z$  axis in the direction normal to the incoming flow (line AB). The local coordinates have  $x$  axis in the direction normal to cylinder axis on the plane ABC,  $y$  axis identical to the  $Y$  axis, and  $z$  axis in the direction of the cylinder axis. The global axes are useful to describe information of incoming flow, and the local coordinates are important for explaining behavior of flow around and forces on the yawed cylinder.

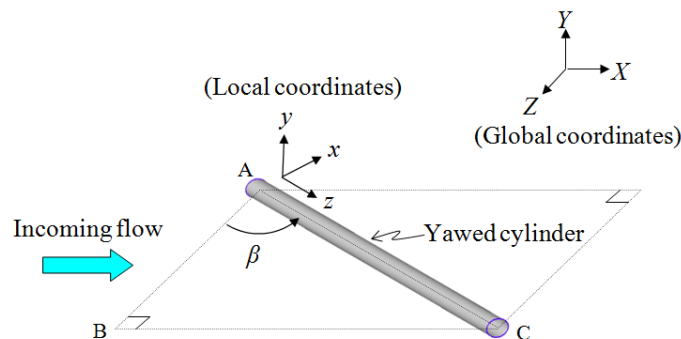


Figure 1. A yawed circular cylinder

### 2.3 Strake patterns

Strake patterns on a circular cylinder investigated in this study are shown in Figure 2. A cylinder of type A has three helical stakes of a  $10D$  pitch with  $10D/3$  interval and  $0.1D$  thickness where  $D$  is the diameter of the cylinder. A cylinder of type B has 12 axial stakes with  $0.05D$  thickness. A type C cylinder has two strake patterns; both have  $10D$  pitches and  $0.1D$  thickness, but their rotation directions are opposite along the cylinder axis.

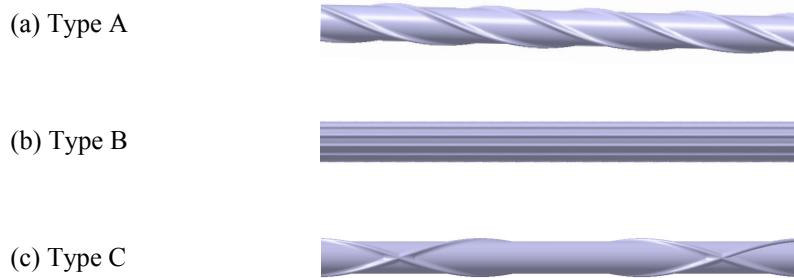


Figure 2. Strake patterns (cylinder length =  $20D$ )

### 2.4 numerical methods

Three-dimensional simulations with the S-A DES model were conducted for a flow past a  $40^\circ$ -yawed cylinder with strakes at  $Re = 1.4 \times 10^5$  (based on freestream velocity  $U$  and the diameter of the cylinder  $D$ ). The computational domain had an extent of  $35D$  in the streamwise direction ( $15D$  in the upstream region and  $20D$  in the downstream region),  $25D$  in the cross-stream direction ( $12.5D$  from the center of the cylinder to the top and bottom side), and the cylinder length of  $10D$  in the spanwise direction (i.e., the local  $z$  axis).

The simulation employed a constant velocity for the upstream boundary, zeroth order extrapolation with fixed static pressure for the downstream boundary, slip wall conditions for the top and bottom boundaries, and periodic boundary conditions for both spanwise wall boundaries. A no-slip condition was used without wall functions on the wall of the cylinder because sufficient grids were assigned in the viscous layer (e.g.,  $\Delta y^+$  of the first grid normal to the wall is near unity where  $\Delta y^+$  is a non-dimensional viscous length scale based on the viscosity and wall shear stress of the flow).

The total number of grid elements was approximately  $1.2 \times 10^6$ . The simulation used 128 nodes on the cylinder surface along the perimeter and 61 nodes of  $0.167D$  interval along the cylinder length. The numerical schemes were a fifth order upwind scheme for convection, a second order central scheme for viscosity, and a two-step MacCormack implicit scheme for time integration with four Newton sub-iterations per timestep. A non-dimensional timestep of 0.01 (calculated as  $\Delta t^* = Ut/D$ ) was used.

The simulation assumed turbulent separation from the cylinder surface due to its turbulent boundary layer generated by the S-A DES model. The characteristics of aerodynamic pressures and forces induced by the turbulent separation in this DES study are in good agreement to those by the upstream incoming flow with moderate level of turbulence intensity. Details of verification and validation associated with this numerical study were provided in Yeo (2008).

### 3 RESULTS OF SIMULATIONS

#### 3.1 Vortex structures

Figure 3 shows vortex flow structures past a yawed cylinder (flow from left to right.) They are described by using the iso-surfaces of the second invariant  $Q = 5000 \text{ [s}^{-2}\text{]}$  from the velocity gradient tensor where its contour range of the vorticity about the cylinder axis (i.e., local  $z$  axis) is from  $-300 \text{ [s}^{-1}\text{]}$  to  $300 \text{ [s}^{-1}\text{]}$  (Hunt et al., 1988).

For a yawed bare cylinder of Figure 3(a), the vortex structures do not shed parallel to the cylinder axis and their axis lines are not linear. Their separation is delayed at locations where intense low pressure is generated by swirling flows that have strong vorticity with axial velocity near the cylinder. The swirling flows, induced by the flow oblique to a cylinder, develop alternately from the upper and the lower surfaces of the cylinder while moving downward along the cylinder. They play a key role in developing the three-dimensional and complex flow oblique to a cylinder (Yeo and Jones, 2008).

For a yawed cylinder with strakes, the strakes disturb development of the vortex flow structures observed in a bare yawed cylinder. In a type A cylinder, for example, vortex flow structures generate differently at the upper and the lower sides of the cylinder. The strakes on the upper side are aligned against the flow path and disturb rolled-up shear layer flow along the oblique cylinder. But those on the lower side are aligned along the flow path and their disturbance of vortex shedding is relatively small. Swirling flow along the cylinder was not seen. In a type B cylinder, two cases were investigated: one (type B(1)) is for symmetric axial strakes along the flow direction, and the other (type B(2)) is for asymmetric strakes where the stakes are rotated by  $7.5^\circ$  along the cylinder axis. For type B(1), vortex flow structures shed alternately from both sides of the cylinder without swirling flow. But, for type B(2), swirling flow structures are detected though their strength is not as great as that of the bare cylinder.

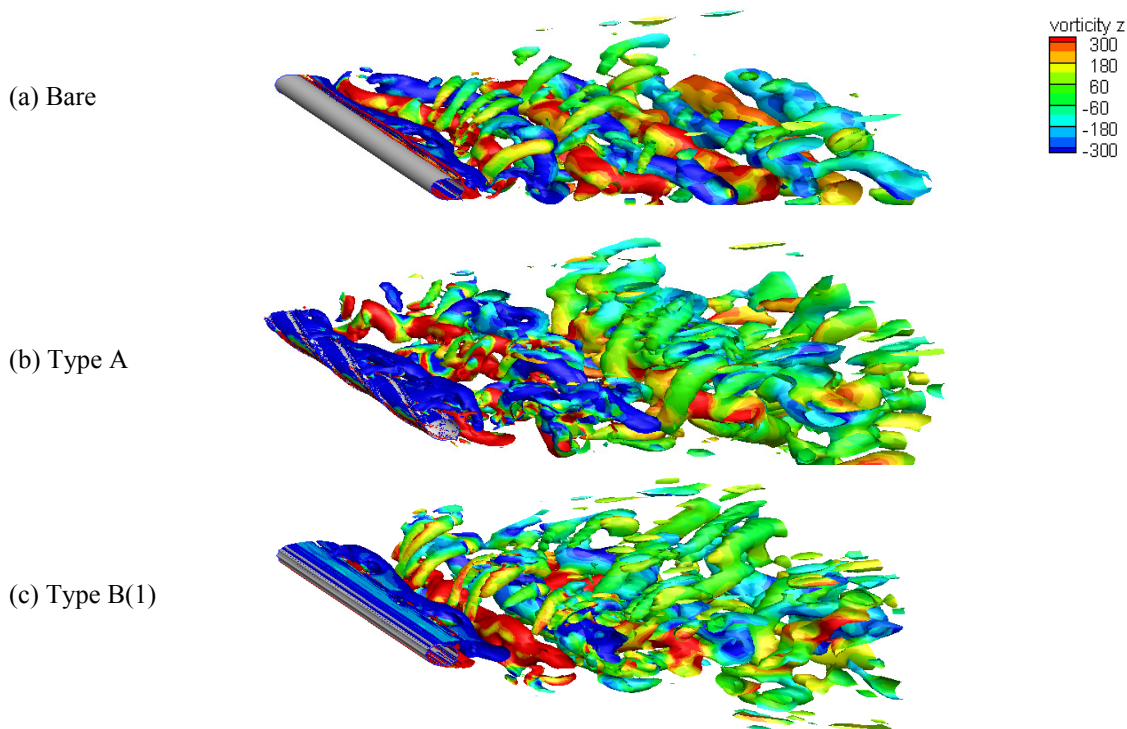


Figure 3. Vortex flow structures around a yawed cylinder

### 3.2 Aerodynamic pressures and forces

This study investigated aerodynamic forces induced by flow around the yaw cylinder with strakes. In order to improve understanding of the effects of strakes, Figure 4 shows spatial-temporal force coefficients of cylinders with and without strakes. The horizontal and vertical axes represent non-dimensional time ( $t^* = Ut/D$ ) and cylinder length ( $z/D$ ) where  $U$  is the upstream velocity of incoming flow,  $t$  is time in dimension, and  $z$  is the length from the upper end of the cylinder along the cylinder axis.

Non-dimensional force coefficients ( $C_x$  and  $C_y$ ) in the local  $x$  and  $y$  axes are defined as

$$C_x = \frac{F_x}{\frac{1}{2}\rho U^2 A}, \quad C_y = \frac{F_y}{\frac{1}{2}\rho U^2 A} \quad (1)$$

where  $F_x$  and  $F_y$  are forces on the cylinder in the  $x$  and  $y$  axes,  $\rho$  is the density of the air, and  $A$  is a horizontally projected area of the cylinder.

The result for a yawed bare cylinder shows that peak forces on the cylinder have a finite length and move downward along the cylinder with time and that the downward speed is approximately 90 % of axial velocity component  $U\sin\beta$  of incoming flow whose velocity is  $U$  (Yeo and Jones, 2008). The moving peak forces due to swirling flow are the main feature of forces on a circular cylinder induced by oblique flow. This mechanism of force generation is valid when a yaw angle is below a critical value where swirling flow structures and mitigated Kármán vortices interact (Yeo and Jones, 2009).

Flow-induced forces on a yawed cylinder with strakes have different distributions in time and space according to their strake patterns. For the strake pattern of type A, three peak forces in the cylinder length have no moving component along the axis, which implies effective disturbance of the three-dimensional force generation as shown in a yawed bare cylinder. But, the strakes significantly increases drag force and fluctuation of lift force. In particular, the time-averaged lift force is negative due to asymmetric strake patterns of upper and lower sides along oblique flow direction. For the strake pattern of type B, two peak forces in type B(1) generate and move downward along the cylinder axis. In type B(2), distribution of peak forces is changed due to the asymmetric strake alignment and one peak forces move along the axis as those for a yawed bare cylinder. For the strake pattern of type C, peak forces do not move along the cylinder axis. Their fluctuations are much smaller than those of type A, and the time-averaged lift force is zero.

Figure 5 compares characteristics of flow induced forces of a yawed cylinder with strake patterns. Obstruction of flow due to strakes increases  $x$ -axis time-averaged forces on all cylinders with the strakes in comparison with those on a bare cylinder. It is noted that the type A pattern has the largest time-averaged forces and fluctuations and that the type C pattern generates the smallest forces among cylinders with strakes.

The frequency distributions of forces ( $C_x$  and  $C_y$ ) are shown in Figure 6 using fast Fourier transform (FFT) to compute the power spectral density (PSD) of the corresponding force coefficients. The ordinate denotes non-dimensional cylinder length ( $L/D$ ), and the abscissa is the non-dimensional reduced frequency ( $f_r = Df/U$ ) where  $f$  is a real frequency of force coefficients with dimension. The plots of  $C_x$  for a yawed cylinder with strakes are not shown in this paper for space limitation.

For a yawed bare cylinder (Figure 6(a)),  $y$ -axis reduced frequencies are distributed in the center of mitigated Kármán vortex shedding frequency ( $f_r = 0.191$ ) at an interval of  $\Delta f_r = 0.059$ . The interval is the same as  $x$ -axis reduced frequency. This is caused by modulation of amplitude and frequency in forces (Yeo and Jones, 2009). Note that the PSD of  $C_y$  has the highest peak at  $f_r = 0.132$ , not at the vortex shedding frequency.

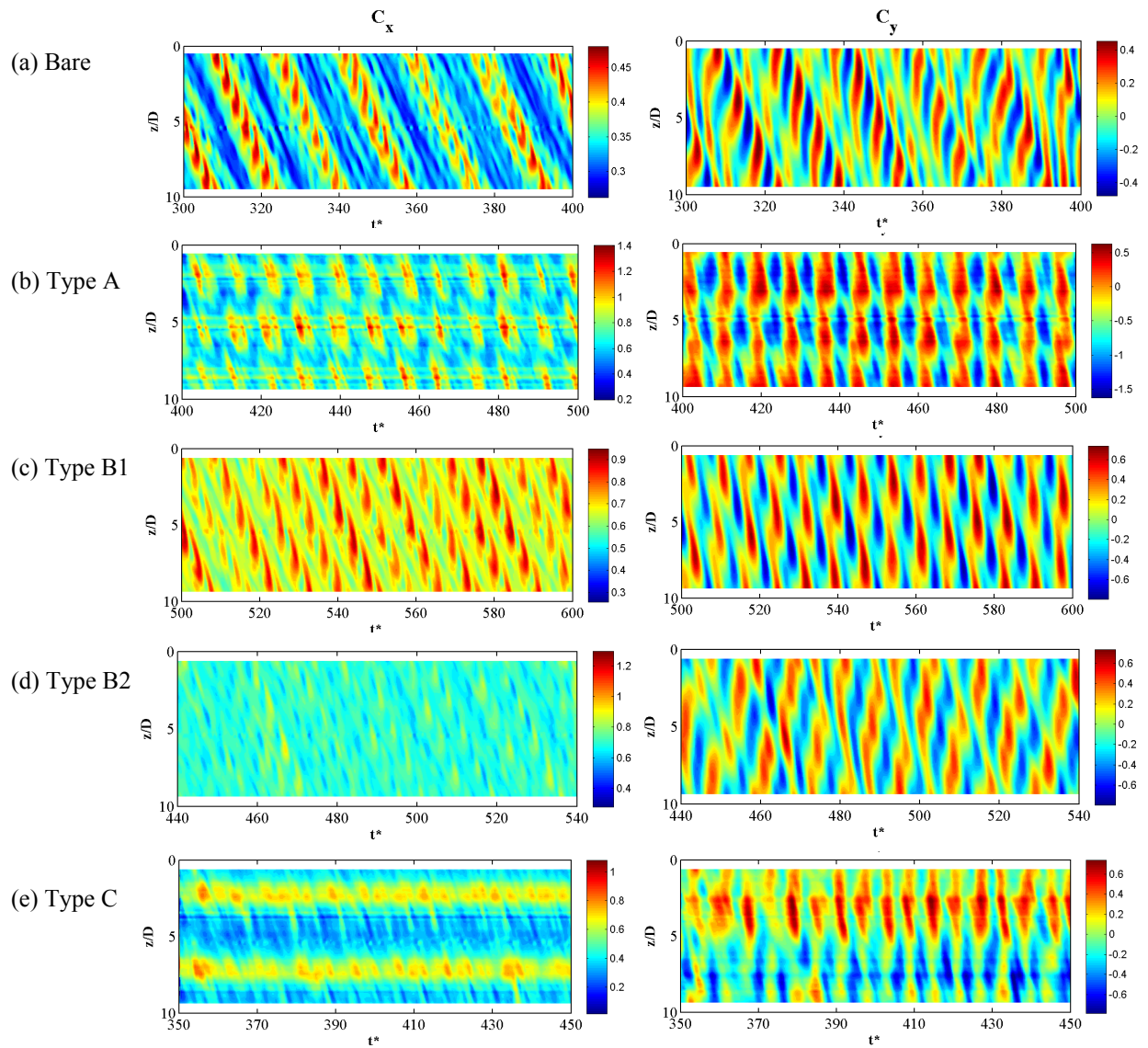


Figure 4. Spatial-temporal force distributions

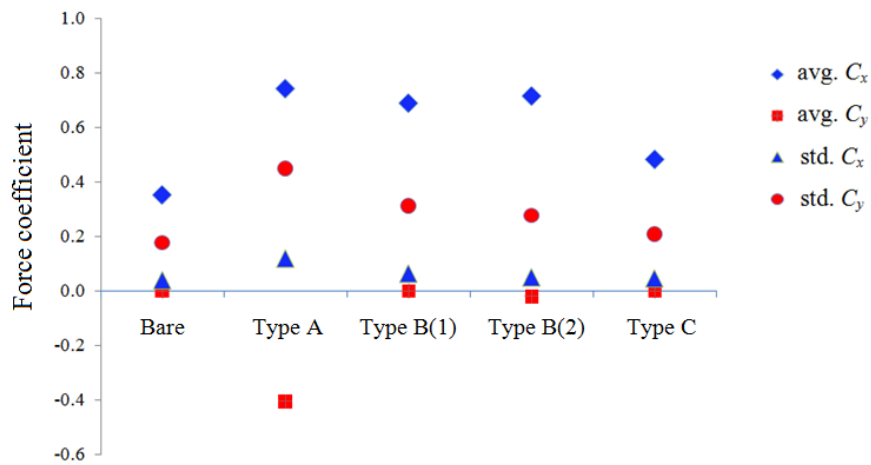


Figure 5. Characteristics of forces on a yawed cylinder

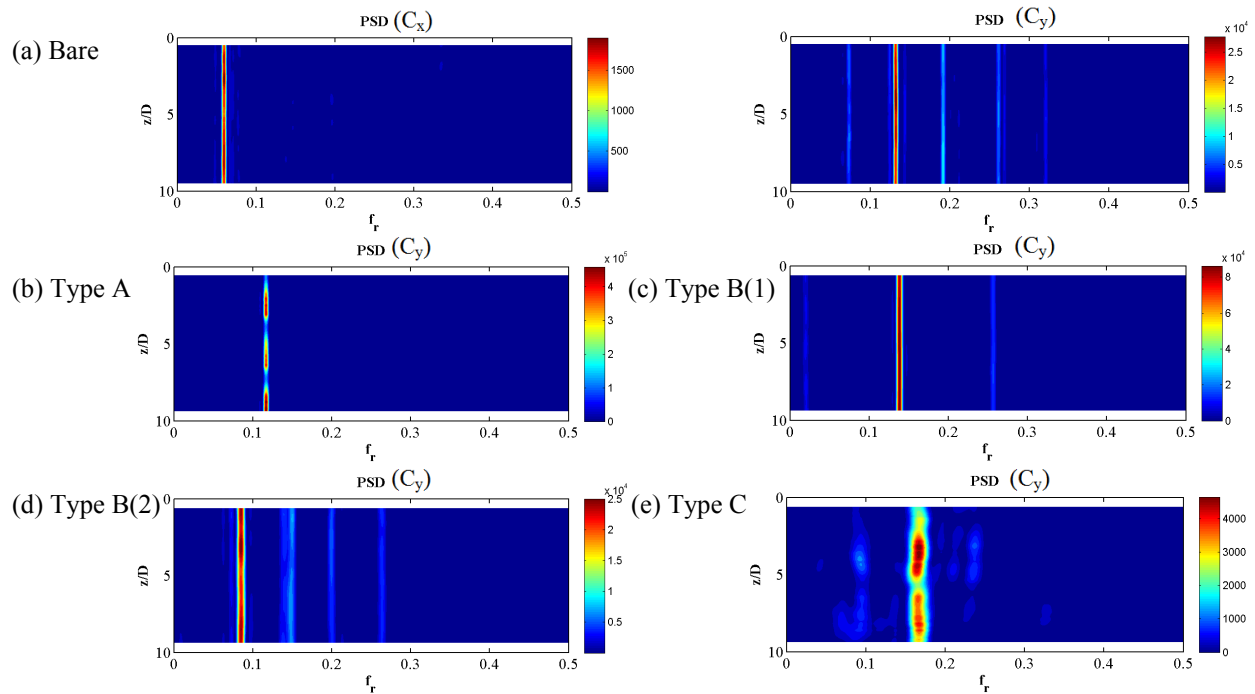


Figure 6. Frequency distribution of forces

For a yawed cylinder with strakes (Figures 6(b) to 6(e)), the frequency distribution depends on the effects of strake patterns. In a type A cylinder, one peak frequency is shown at  $f_r = 0.117$  for both  $x$  and  $y$  axes, and no low frequency component exists. In a type B cylinder, when the axial strakes are asymmetrically aligned along flow direction (i.e., type B(2)), the  $y$ -axis frequencies are distributed by equi-interval and has a peak at low frequency, which is similar to those of the yawed bare cylinder (Figure 6 (c)). It implies that the inherent three-dimensional flow is still developed along the cylinder. In a type C cylinder, the  $y$ -axis peak frequency is 0.167 and  $x$ -axis peak ones are scattered. Note that the PSD of  $C_y$  at the peak frequency is much lower than those for the other strake patterns.

According to these results, the type C strake pattern shows good performance in suppressing Kármán vortex shedding and therefore the three dimensional flow structures among the three strake patterns employed in this study. However, further study is recommended for better understanding the true effectiveness of strake patterns, considering factors such as asymmetric alignment of strakes to flow direction, pitch, and shape of strakes

#### 4 CONCLUSIONS

Three-dimensional DES flow around a  $40^\circ$  yawed cylinder with various strake patterns was studied. Effects of the strake patterns on flow around and the associated forces on the cylinder were investigated and compared to inherent aerodynamic characteristics of a yawed bare cylinder. Frequency distributions of the forces were examined to investigate how the strake patterns effectively disturb or suppress the inherent mechanism of force generation along a cylinder oblique to flow.

Results showed that a suitable strake pattern enables disturbance of the development of inherent flow structures around an oblique cylinder. It consequently suppresses or weakens the associated forces at low frequency on the cylinder as a potential excitation source for large-amplitude and low-frequency vibrations. Because the flow-induced forces on an oblique bare cylinder develop using modulation mechanism under mitigated Kármán vortex flow structures, an aerodynamic countermeasure for suppression of the Kármán vortex flow structures appears to be effective.

## 5 REFERENCES

- Hikami, Y., Shiraishi, N., 1988. Rain-wind induced vibrations of cables stayed bridges. *Journal of Wind Engineering and Industrial Aerodynamics* 29(1-3), 409-418.
- Hunt, J.C.R., Wray, A.A., Moin, P., 1988. Eddies, stream, and convergence zones in turbulent flows. Report CTR-S88, Center for Turbulence Research.
- Larose, G.L., Savage, M.G., Jakobsen, J.B., 2003. Wind tunnel experiments on an inclined and yawed circular cylinder in the critical Reynolds number range, in: *Proceedings of the 11th International Conference on Wind Engineering*, Lubbock, Texas, 1705-1712.
- Main, J.A., Jones, N.P., 1999. Full-scale measurements of stay cable vibration, in: *Proceedings of the 10th International Conference on Wind Engineering*, Copenhagen, Denmark, 963-970.
- Matsumoto, M., 1998. Observed behavior of prototype cable vibration and its generation mechanism, in: *Proceedings of the Advances in Bridge Aerodynamics*, Balkema, Rotterdam, The Netherlands, 189-211.
- Matsumoto, M., Daito, Y., Kanamura, T., Shigemura, Y., Sakuma, S., Ishizaki, H., 1998. Wind-induced vibration of cables of cable-stayed bridges. *Journal of Wind Engineering and Industrial Aerodynamics* 74-76, 1015-1027.
- Miyata, T., Yamada, H., Hojo, T., 1994. Aerodynamic response of PE stay cables with pattern indented surface, in: *Proceedings of the the IABSE/FIP International Conference on Cables-Stayed and Suspension Bridges*, Deauville, 515-522.
- Spalart, P.R., 2000. Strategies for turbulence modelling and simulations. *International Journal of Heat and Fluid Flow* 21(3), 252-263.
- Spalart, P.R., Allmaras, S.R., 1992. A one-equation turbulence model for aerodynamic flows, in: *Proceedings of the 30th Aerospace Sciences Meeting and Exhibit*, Reno, NV, 1-22.
- Spalart, P.R., Jou, W.H., Strelets, M., Allmaras, S.R., 1997. Comments on the feasibility of LES for wings, and on a hybrid RANS/LES approach, in: *Proceedings of the Advances in DNS/LES, 1st AFOSR International Conference on DNS/LES*, Ruston, LA, 137-147.
- Verwiebe, C., Ruscheweyh, H., 1998. Recent research results concerning the exciting mechanisms of rain-wind-induced vibrations. *Journal of Wind Engineering and Industrial Aerodynamics* 74-76, 1005-1013.
- Yeo, D., 2008. Numerical simulation of 3-D aerodynamic behavior of a yawed, inclined circular cylinder University of Illinois at Urbana-Champaign, Urbana.
- Yeo, D., Jones, N.P., 2008. Investigation on 3-D characteristics of flow around a yawed and inclined circular cylinder. *Journal of Wind Engineering and Industrial Aerodynamics* 96(10-11), 1947-1960.
- Yeo, D., Jones, N.P., 2009. A mechanism for large amplitude, wind-induced vibrations of stay cables, in: *Proceedings of the Eleventh Americas Conference on Wind Engineering*, San Juan, Puerto Rico.